PPP2R3C gene variants cause syndromic 46,XY gonadal dysgenesis and impaired spermatogenesis in humans

Tulay Guran[1], Gozde Yesil[2], Serap Turan[1], Zeynep Atay[3], Emine Bozkurtlar[4], AghaRza Aghayev[5], Sinem Gul[6], Ilker Tinay[7], Basak Aru[8], Sema Arslan[9], M Kutay Koroglu[10], Feriha Ercan[10], Gulderen Y Demirel[8], Funda S Eren[4], Betul Karademir[9] and **Abdullah Bereket[1]**

[1]Department of Paediatric Endocrinology and Diabetes, Marmara University, [2]Department of Genetics, Bezm-i Alem University, [3]Department of Paediatric Endocrinology and Diabetes, Medipol University, [4]Department of Pathology, Marmara University, School of Medicine, Istanbul, Turkey, [5]Department of Medical Genetics, Istanbul Faculty of Medicine, Istanbul University, Istanbul, Turkey, [6]Department of Molecular Biology and Genetics, Gebze Technical University, Kocaeli, Turkey, [7]Department of Urology, Marmara University, School of Medicine, Istanbul, Turkey, [8]Department of Immunology, Yeditepe University, Faculty of Medicine, Istanbul, Turkey, [9]Department of Biochemistry, Genetic and Metabolic Diseases Research and Investigation Center, and [10]Department of Histology and Embryology, Marmara University, School of Medicine, Istanbul, Turkey

Correspondence should be addressed to T Guran
Email
tulayguran@yahoo.com

European Journal of Endocrinology

Abstract

Context: Most of the knowledge on the factors involved in human sexual development stems from studies of rare cases with disorders of sex development. Here, we have described a novel 46, XY complete gonadal dysgenesis syndrome caused by homozygous variants in *PPP2R3C* gene. This gene encodes B″gamma regulatory subunit of the protein phosphatase 2A (PP2A), which is a serine/threonine phosphatase involved in the phospho-regulation processes of most mammalian cell types. *PPP2R3C* gene is most abundantly expressed in testis in humans, while its function was hitherto unknown.

Patients and methods: Four girls from four unrelated families with 46, XY complete gonadal dysgenesis were studied using exome or Sanger sequencing of *PPP2R3C* gene. In total, four patients and their heterozygous parents were investigated for clinical, laboratory, immunohistochemical and molecular characteristics.

Results: We have identified three different homozygous *PPP2R3C* variants, c.308T>C (p.L103P), c.578T>C (p.L193S) and c.1049T>C (p.F350S), in four girls with 46, XY complete gonadal dysgenesis. Patients also manifested a unique syndrome of extragonadal anomalies, including typical facial gestalt, low birth weight, myopathy, rod and cone dystrophy, anal atresia, omphalocele, sensorineural hearing loss, dry and scaly skin, skeletal abnormalities, renal agenesis and neuromotor delay. We have shown a decreased SOX9-Phospho protein expression in the dysgenetic gonads of the patients with homozygous *PPP2R3C* variants suggesting impaired SOX9 signaling in the pathogenesis of gonadal dysgenesis. Heterozygous males presented with abnormal sperm morphology and impaired fertility.

Conclusion: Our findings suggest that PPP2R3C protein is involved in the ontogeny of multiple organs, especially critical for testis development and spermatogenesis. PPPR3C provides insight into pathophysiology, as well as emerging as a potential therapeutic target for male infertility.

European Journal of Endocrinology
(2019) **180**, 291–309

https://eje.bioscientifica.com
https://doi.org/10.1530/EJE-19-0067

Published by Bioscientifica Ltd.

Introduction

Human sex development is an active molecular signaling cascade that orchestrates the interaction of agonistic and antagonistic effectors at a sufficient dosage and in a delicate spatiotemporal order, beginning around the sixth gestational week (1). This pathway transforms an initially bipotential gonad into an ovary or a testis. Disorders of sex development (DSD) result from the disruption of these processes, often due to genetic mutations in the key molecules within these pathways, which subsequently alter developmental programming and sex hormone production and cause atypical development of internal and external genital structures. This group of congenital conditions are generally associated with impaired process of reproduction and consequently with infertility. Most of the knowledge on the factors involved in human sexual development stems from studies of rare cases with DSD. The identification of a genetic diagnosis for DSDs promises to further our understanding of human development and reproduction, improves personalized management particularly about sex or rearing, time and type of genital surgeries, hormone treatments, interventions for reproduction, genetic counseling and better predicts patient outcomes for a lifelong care (2). New genetic and genomic technologies such as array-comparative genomic hybridization (aCGH) and whole-exome sequencing revealed new causes of DSD and expanded our knowledge in the molecular mechanisms underlying gonadal development. However, the genetic etiology remains unidentified in the majority of DSD cases (3, 4).

Here, we identify three different homozygous missense variants in the gene encoding protein phosphatase two regulatory subunit B″gamma, *PPP2R3C* (synonyms; C14orf10, FLJ20644, G4-1, G5PR) as the cause of a novel syndromic 46, XY gonadal dysgenesis in four females from four independent consanguineous families. Human *PPP2R3C* is located in Chr. 14q13.2 (OMIM: 615902; Genomic coordinates (GRCh38): 14:35, 085, 466-35, 122, 661), which has 13 exons encoding a 453 amino acid protein. Together with scaffolding A and catalytic C subunits, PPP2R3C regulatory subunit protein (type B″) constitutes a heterotrimeric protein phosphatase 2A (PP2A) which is an important intracellular signaling molecule involved in the reversible dephosphorylation of phospho-proteins within a mutual relation with protein kinases. In humans, there are 16 regulatory B subunits including PPP2R3C, which were allocated in the diverse cellular processes (5). The only known *in vivo* function of *PPP2R3C* gene comes from the homozygous conditional and targeted knockout mice for this gene, which exhibit impaired survival of B lymphocytes and increased B lymphocyte receptor-induced apoptosis (6, 7). However, germline genetic defects in *PPP2R3C* in humans is of unknown functional significance. This report gives the first insights about the pivotal role of PPP2R3C on human development.

Subjects and methods

Clinical studies

All clinical investigations and genetic analyses were performed according to the guidelines of the Declaration of Helsinki and with written consent of the families. The Ethical Committee of Marmara University, Istanbul, Turkey approved the study (09.2017.471).

Four female patients from four independent consanguineous families were evaluated for a syndromic 46, XY gonadal dysgenesis with common syndromic features at different times between 2012-2018. Detailed clinical, laboratory and molecular characteristics of the patients and families are described.

Whole-exome sequencing (WES)

Genomic DNA was extracted from peripheral blood using MagnaPure X blood extraction kit according to standard protocols (Roche Diagnostics). WES was performed for the Patients 1 and 2 using Nextera Rapid Capture Enrichment (Illumina) kit. For each subject, 50 ng of genomic DNA were used to prepare a captured library that was then sequenced on a NextSeq500 platform (Illumina) generating 150 bp paired-end reads. Raw data of approximately 10 GB per exome were mapped to a human reference genome sequence (GRCh37/hg19) using the Burrows–Wheeler Alignment (BWA) tool (8). Variant calling was performed using the Genome Analysis Toolkit (GATK) (9). All variants were further annotated with ANNOVAR software (10).

Variant frequency was evaluated with public databases such as Exome Aggregation Consortium (ExAC), 1000 Genomes Project and GnomAD (11). For functional prediction of single-nucleotide variants (SNVs) SIFT (12), PolyPhen-2 (13) and MutationTaster (14) databases were used. Since we observed a new phenotype, therefore, expect a novel gene, candidate genes were evaluated on the basis of OMIM, Uniprot, Genecards, NCBI databases.

Sanger sequencing

All the coding exons and intron–exon boundaries of the *PPP2R3C* gene were amplified by PCR. Primers were designed using Primer3 software (http://www.bioinformatics.nl/cgi-bin/primer3plus/primer3plus.cgi). Primer sequences were as follows: PPP2R3C_E4_1F: 5′-CAGCCCTGCTATATGACTTTAGGCA-3′, PPP2R3C_E4_2R: 5′-CTTACTTGCACTTTGCTCCAGCCT-3′, PPP2R3C_E4_3F: 5′-TCTGCCAACAAACTCTCATTTTAGTG-3′, PPP2R3C_E7_1F: 5′-TGCATCTGTTACCTTTGGGAAGC-3′, PPP2R3C_E7_2R: 5′-AGAACTTCCTAACTGCTGTACAAACAT-3′, PPP2R3C_E7_3F: 5′-CCACTAAAATAGTCATGCATTTATTTCT-3′, PPP2R3C_E7_4R: 5′-CAGACCATCTAATTGTGGCAACG-3′, PPP2R3C_E11_1F: 5′-CCACCTTTGATTGCAAAATAGCTTC-3′, PPP2R3C_E11_2R: 5′-CAGGATGGTCTCTATCTCCTGACCT-3′, PPP2R3C_E11_3F: 5′-TCAACTAAGGCCTCTAATGAACAT-3′, PPP2R3C_E11_4R: 5′-CTCCCAAAGTGCTGGGATTACA-3′.

The reaction mixture contained 100 ng DNA template, 1× PCR buffer, 200 µM each dNTP, 200 nM each primer, and 1 U Taq DNA polymerase (Thermo Scientific). Cycling conditions were as follows: 95°C for 5 min (1 cycle); 95°C for 30 s, 55°C for 45 s and 72°C for 60 s (34 cycles) and 72°C for 10 min. PCR products were visualized on 1% agarose gel and were purified using the ExoSAP-IT (GE Healthcare Bio-Sciences), following the manufacturer's protocol. Sequence reactions were run on an ABI Prism 3130*xl* DNA Sequencer and analyzed by Seqscape sequencing analysis software, version 2.7 (Applied Biosystems).

Quantitative PCR (qPCR)

Total RNA was extracted from peripheral blood using the PureLink RNA purification kit (Thermo Fisher) and reversely transcribed using iScript cDNA synthesis kit, according to manufacturers' instructions. The sequences for qPCR primers were as follows: PPP2R3C_E4_3F: 5′-TCTGCCAACAAACTCTCATTTTAGTG-3′, PPP2R3C_E4_2R: 5′-CTTACTTGCACTTTGCTCCAGCCT-3′, PPP2R3C_E7_3F: 5′-CCACTAAAATAGTCATGCATTTATTTCT-3′, PPP2R3C_E7_4R: 5′-CAGACCATCTAATTGTGGCAACG-3′, PPP2R3C_E11_3F: 5′-TCAACTAAGGCCTCTAATGAACAT-3′, PPP2R3C_E11_4R: 5′-CTCCCAAAGTGCTGGGATTACA-3′; GAPDH_F: 5′-GAGTCAACGGATTTGGTCGT-3′, GAPDH_R: 5′-TTGATTTTGGAGGGATCTCG-3′. The qPCR reactions were performed with the power SYBR green PCR Master Mix (BioRad) and run on a Rotor-Gene Q Real-Time System (Qiagen). Expression levels were calculated using the ΔΔCt method relative to the GAPDH control gene.

Protein modeling

Three-dimensional models for the full PPP2R3C protein and three coding mutants (p.Pro103, p.Ser193 and p.Ser350) were created based on multiple-threading alignments by Local Meta-Threading-Server (LOMET) using *in silico* tool, I-TASSER (http://zhanglab.ccmb.med.umich.edu/I-TASSER). I-Tasser builds five predictions with individual confidence scores estimating the quality of the models based upon the capacity of the threading template alignments and the convergence parameters of the structure assembly simulations. Typically, the confidence score of 3D models in this system ranges between −5 and +2, where the higher value signifies greater confidence. Alterations of the solvent accessibility were observed, 3D models are visualized at PyMol viewer and secondary structures were investigated.

Histopathology and immunohistochemistry

The paraffin blocks of the gonadal tissues were cut at 2 µ thick sections, one slide was stained with hematoxylin-eosin (H&E) for histomorphological evaluation. The sections of immunohistochemical procedure were incubated at 60°C for 1 h on the adhesive slides. All the slides were stained in Ventana Medical System-Benchmark Ultra/ISH^{TR} staining machine and ultraView Universal DAB Detection Kit (Roche^{TR}) was applied. Antigen retrieval was performed with EDTA for inhibin (Leica^{TR}), PPP2R3C (Thermo fisher^{TR}), SOX9-Phospho (Abbkine^{TR}) and, with citrate for SOX9 (Epitomics^{TR}). The concentration of inhibin, PPP2R3C, SOX9 and SOX9-Phospho antibodies were 1/100. After primary antibody treatment, slides were stained in Harris Hematoksilen (Ventana^{TR}) for 16 min to get background staining and, finally were washed in water, dehydrated in alcohol and mounted.

Sperm analysis and morphologic evaluation

Ejaculates were obtained from the fathers of the Patients 1, 3 and 4. A routine density gradient method was used to evaluate the spermatozoa. The supernatant was removed and the pellet was diluted with spermatozoa-washing medium (SAGE, UK) and centrifuged. Then the pellet was diluted with sperm preparation medium (SAGE). Ten micrometers of pellet were used to observe the motility and

the number of spermatozoa in a Macler Counting Chamber (Sefi cut out Medical Instruments, Haifa, Israel) with a photomicroscope. Smears were prepared and stained with Diff-Quick kit (Medion Diagnostics, Grafelfing, Germany) for morphologic assessment. One hundred spermatozoa were scored for head, neck and tail morphology at 1000× magnification on a photomicroscope.

Evaluation of B lymphocyte viability, proliferation rate and apoptosis

For flow cytometric assessment of B lymphocyte viability and proliferation rate in a time-dependent manner, erythrocytes were first depleted by incubating 2 mL whole blood in 10 mL ammonium chloride lysis solution at room temperature for 20 min. Isolated mononuclear cells were cultured in RPMI 1640 medium (Sigma Aldrich) containing 10% fetal bovine serum (Gibco, Thermo Fisher Scientific), 1% glutamine (Gibco, Thermo Fisher Scientific) and 1% Penicillin-Streptomycin antibiotic solution (Thermo Fisher Scientific). Analyses were performed on three time points including arrival (hour 0), 24th and 48th h. Cells were stained with CD19-PE antibody (Biolegend, USA), followed by either labeling with Annexin V-FITC (BioVision Inc) and propidium iodide (Thermo Fisher Scientific) or evaluating DNA content by DNA Prep Kit (Beckman Coulter). Samples of six age-matched healthy children (three males and three females) were used as control for comparing viability and apoptosis ratios. Samples were analyzed with Beckman Coulter FC500 flow cytometry. Overall, 50 000 events for Annexin V/PI staining and 100 000 events for DNA content analysis were counted. Analyses were performed with CXP software.

Statistics

Shapiro–Wilks test was used to determine whether the data are normally distributed. When comparing patient data according to timepoints, one-way ANOVA, followed by Tukey's multiple comparisons test was used for parametric values, whereas Kruskal–Wallis followed by Dunn's multiple comparisons test was used for non-parametric values. Two-way ANOVA, followed by Bonferroni's multiple comparisons test, was used for comparing differences between patients and healthy controls. *P* values less than or equal to 0.05 were considered as significant. Data are presented as mean ± S.D. in all figure parts in which error bars are shown.

Results

Case reports

All four female patients were evaluated for 46, XY complete gonadal dysgenesis. They had a female external genitalia with hypoplastic labia majora and clitoris. All had a hypoplastic uterus seen in ultrasound or laparoscopy. In addition to complete gonadal dysgenesis, they shared unique dysmorphic features and major extra gonadal multisystem abnormalities (Fig. 1 and Table 1). In the common facial gestalt; all four patients had flat face, flat vertex, unusual scalp hair whorls, unruly scalp hair, frontal upsweep, arched and sparse eyebrows, bilateral epicanthal folds, thin lips, long and smooth philtrum and hypodontia. All had hypoplastic ala nasi and beaked nose. The oldest patient (patient 3) had an angulated nasal bridge, giving the 'squashed down' appearance, which may be due to nasal cartilage weakness. The patients had also low set and posteriorly rotated ears, overfolded helix, narrowed and elongated intertragic notch with or without sinus. The placement of sinus when present was just under the tip of the intertragal angle, which can be regarded as a pathognomonic finding of the syndrome (Supplementary Fig. 1, see section on supplementary data given at the end of this article). Short and broad hands, a horizontal single crease, cutaneous syndactyly (interphalangeal webbing) in hands were present in all patients (Supplementary Fig. 1). All patients had myopathy and significantly muscular build with thick and stiff muscles particularly in the neck (Supplementary Fig. 1). They had significantly delayed bone ages and some more skeletal abnormalities (Supplementary Fig. 1). Additionally, they had some common growth, skin, gastrointestinal, renal and cardiac abnormalities and neuromotor delay and mental retardation (Table 1). Further clinical characteristics of patients and their families were as follows:

Family 1

A four-month-old female (Patient 1) was referred to our clinic for 46, XY gonadal dysgenesis. History revealed that the pregnancy was achieved by *in vitro* fertilization (IVF) after 6 years of marriage and she was born as a twin sister to first-degree cousin parents at 30th gestation week with 1400 g birth weight (Fig. 1). Her 34-year-old, 155.8 cm mother and 36-year-old, 171 cm father were not chronically exposed to medications, alcohol or cigarette. Patient 1 had several dysmorphic features and multisystem disorders noticed in 2-year clinical follow-up (Fig. 1B

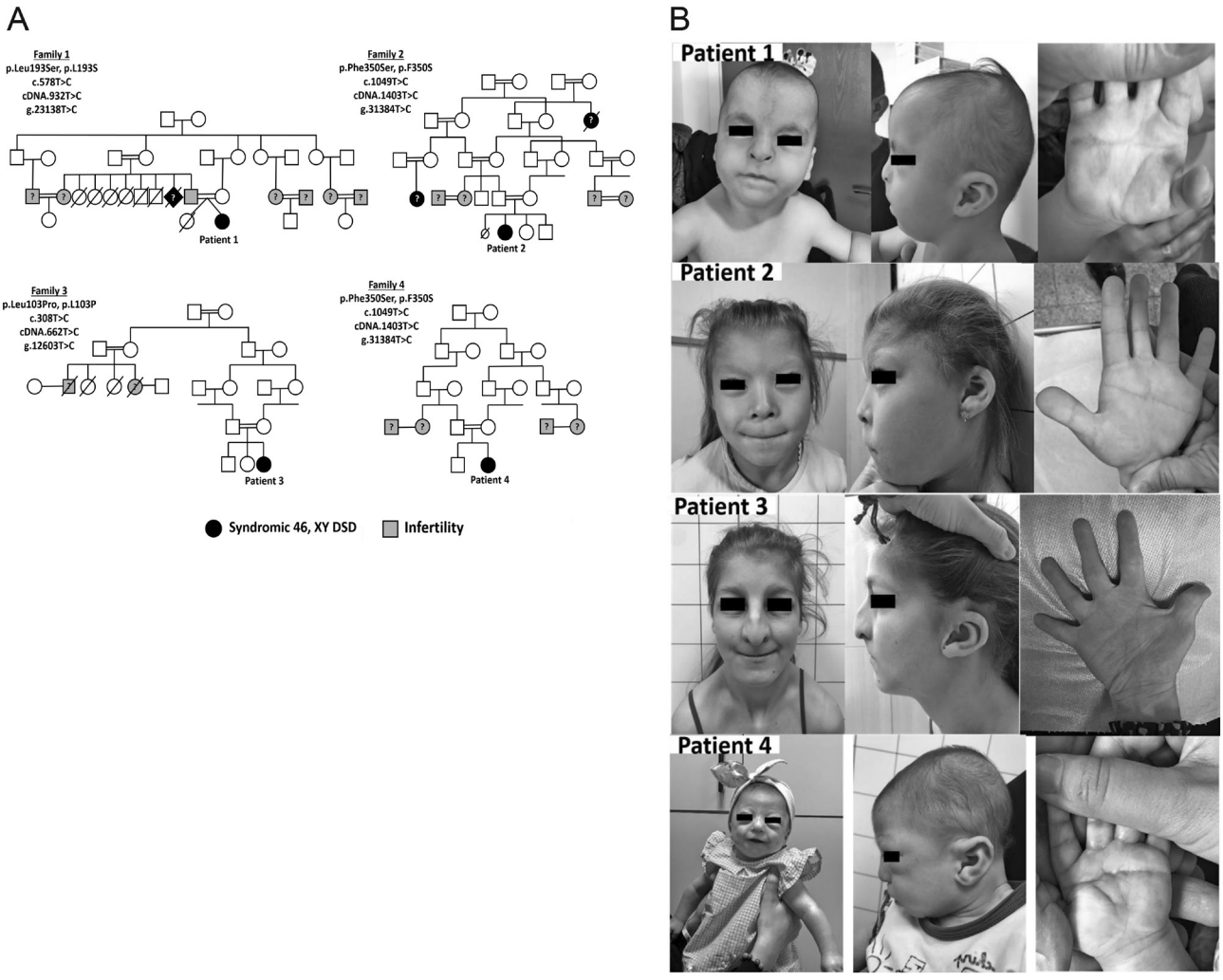

Figure 1

Pedigrees and clinical characteristics of patients with syndromic 46, XY gonadal dysgenesis. (A) Pedigrees of families 1–4 where all affected individuals manifested syndromic 46, XY complete gonadal dysgenesis, and were positive for mutations in *PPP2R3C*. Black symbols indicate individuals with syndromic 46, XY complete gonadal dysgenesis, gray symbols indicate those who had been stated to be infertile. All affected individuals were homozygous for the indicated variants (patients sequenced have been numbered from 1 to 4), and parents were heterozygous. Variants for patients 1 and 2 were identified by WES and the remainder by Sanger sequencing of *PPP2R3C*. The symbols with '?' indicate suggestive clinical phenotype but no further biochemical or genetic data about that individual. (B) Phenotypic features of the patients with syndromic 46, XY gonadal dysgenesis due to homozygous variants in *PPP2R3C*. Pictures at each row belong to the respective patient numbered at upper left corner of each row. The characteristic facial gestalt includes flat face, flat vertex, unusual scalp hair whorls, unruly scalp hair, frontal upsweep, arched and sparse eyebrows, bilateral epicanthal folds, thin lips, hypoplastic ala nasi and beaked nose, long and smooth philtrum, hypodontia, posteriorly rotated and low set ears, overfolded helix, narrowed and elongated intertragic notch with or without a sinus under the tip of the intertragal angle common to all four patients. Muscular habitus with thick and stiff muscles, short and broad hands, a horizontal single palmar crease and interphalangeal webbing are apparent in each patient.

and Table 1). Her karyotype was 46, XY with complete female external genitalia. Her hormonal evaluation was compatible with complete gonadal dysgenesis. Her adrenal functions were normal except some low/normal concentrations of adrenal sex steroids. She had high serum creatine kinase concentrations. Detailed gonadal and adrenal function tests and clinically significant laboratory test results are presented in Supplementary Table 1. At

Table 1 Clinical features of patients with syndromic 46, XY gonadal dysgenesis due to *PPP2R3C* gene variants.

Feature	Patient 1	Patient 2	Patient 3	Patient 4
Karyotype	46, XY	46, XY	46, XY	46, XY
SRY	+	+	+	+
Gonadal phenotype	Complete gonadal dysgenesis	Complete gonadal dysgenesis	Complete gonadal dysgenesis	Complete gonadal dysgenesis
Genital phenotype	Complete female with hypoplastic labium major. Uterus (+)	Complete female with hypoplastic labium major. Uterus (+)	Complete female with hypoplastic labium major. Primitive bicornate uterus (+)	Complete female with hypoplastic labium major. Uterus (+)
Gestational age/birth weight	30 gw/1400 gr	Term/1750 gr	Term/2800 gr	Term/1900 gr
Facial dysmorphism	Flat face, flat vertex, unusual hair whorls, unruly scalp hair, frontal upsweep, arched and sparse eyebrows, narrow forehead with metopic ridge, bilateral epicanthal folds, thin lips, narrow mouth opening, hypoplastic ala nasi and beaked nose, mild "squashed down" appearance of nose, long and smooth philtrum, low set and posteriorly rotated ears, overfolded helix, narrowed and elongated intertragic notch with a sinus under the tip of the intertragal angle	Flat face, flat vertex, unusual hair whorls, unruly scalp hair, frontal upsweep, arched and sparse eyebrows, bilateral epicanthal folds, thin lips, narrow mouth opening, hypoplastic ala nasi and beaked nose, long and smooth philtrum, hypodontia, low set and posteriorly rotated ears, overfolded helix, narrowed and elongated intertragic notch with a sinus under the tip of the intertragal angle	Flat face, flat vertex, unusual hair whorls, unruly scalp hair, frontal upsweep, arched and sparse eyebrows, bilateral epicanthal folds, thin lips, narrow mouth opening, hypoplastic ala nasi and beaked nose, "squashed down" appearance of nose, long and smooth philtrum, hypodontia, low set and posteriorly rotated ears, overfolded helix, narrowed and elongated intertragic notch with a sinus under the tip of the intertragal angle	Flat face, flat vertex, unusual hair whorls, unruly scalp hair, frontal upsweep, arched and sparse eyebrows, narrow forehead with metopic ridge, bilateral epicanthal folds, thin lips, narrow mouth opening, hypoplastic ala nasi and beaked nose, long and smooth philtrum, low set and posteriorly rotated ears, overfolded helix, narrowed and elongated intertragic notch
Ocular	Rod cone dystrophy, lacrimal puncta hypoplasia	Rod cone dystrophy, iris coloboma, lacrimal puncta hypoplasia	Rod cone dystrophy, lacrimal puncta hypoplasia	Rod cone dystrophy, lacrimal puncta hypoplasia
Hand	Short, broad hands, a horizontal single crease, interphalangeal webbing	Short, broad hands, a horizontal single crease, interphalangeal webbing	Short, broad hands, a horizontal single crease, interphalangeal webbing	Short, broad hands, a horizontal single crease, interphalangeal webbing
Muscle system	Severe myopathy, thick/stiff muscles, muscular habitus	Severe diffuse myopathy in electromyography, thick/stiff muscles, muscular habitus	Severe diffuse myopathy in electromyography, thick/stiff muscles, muscular habitus	Severe myopathy, thick/stiff muscles, muscular habitus
Auditory	Not available	Sensorineural hearing loss	Sensorineural hearing loss	Normal auditory brain response audiometry, acoustic immittance and distortion product otoacoustic emissions test
Skeletal system	Delayed bone age, limited elbow extension	Delayed bone age, bifid distal phalanx of toe and thumb, limited elbow extension, short stature	Delayed bone age, hip dysplasia, scoliosis, pectus excavatum, narrow thorax, limited elbow extension	Delayed bone age, limited elbow extension
Cardiac defect	None	None	None	Bicuspit aorta, mild aortic stenosis
Skin	Dry and scaly skin	Dry and scaly skin	Dry and scaly skin	Dry and scaly skin

Table 1 Continued.

Feature	Patient 1	Patient 2	Patient 3	Patient 4
Gastrointestinal system	–	Omphalocele	Diastasis recti, accessory spleen	Anal atresia, pyloric stenosis, omphalocele
Urinary system	–	–	Unilateral renal agenesis	Unilateral renal agenesis
Neurocognitive function and cranial MRI findings	Neuromotor delay, plaques in bilateral ventricular ependyma and punctate calcifications in cranial MRI	Neuromotor delay, agenesis of corpus callosum in cranial MRI	Neuromotor delay	Neuromotor delay
Genetic defect identified in *PPP2R3C* gene	p.Leu193Ser, p.L193S c.578T>C cDNA.932T>C g.23138T>C (Homozygous)	p.Phe350Ser, p.F350S c.1049T>C cDNA.1403T>C g.31384T>C (Homozygous)	p.Leu103Pro, p.L103P c.308T>C cDNA.662T>C g.12603T>C (Homozygous)	p.Phe350Ser, p.F350S c.1049T>C cDNA.1403T>C g.31384T>C (Homozygous)

her last visit, she was $2^{3/12}$ years of age, weighted 11.9 kg (3–10%), was 87.5 cm tall (50–75%) and had a 47.8 cm head circumference (3%). Her span was 7.5 cm less than her height (between −1 and −2 SDS) and her upper/lower ratio was 1.3 (normal for age is <1.23). Her dichorionic diamniotic twin sister survived 4 h postnatally and had multiple congenital anomalies including tetramicromelia, narrow thorax, brachycephaly, bilateral lagophthalmos, punctate corneal staining, severe systolic cardiac dysfunction and bilateral cystic encephalomalacia in cranial parietal lobes. Three more relative couples in the family were reported to be infertile and had healthy children after 6–12 years of their marriages by IVF. They were unavailable for further investigation. One paternal sibling of Patient 1 was said to have 'no external genitalia' to be described as male or female. This infant died at 6 months of age due to an unknown etiology. The father of Patient 1 had 6 more deceased sibs before 1 year of age for unknown reasons, who were mostly stated as females.

Family 2

$3^{7/12}$ years old female (Patient 2) was referred to our clinic for 46, XY gonadal dysgenesis. She was born to consanguineous parents at term with 1750 g birth weight (Fig. 1A). Her 27-year-old, 153.5 cm mother and 31-year-old, 174.2 cm father were well. Patient 2 had several dysmorphic features and multisystem disorders similar to Patient 1 noticed in 6.5-year clinical follow-up (Fig. 1B and Table 1). Her karyotype was 46, XY with complete female external genitalia. Her hormonal evaluation was compatible with complete gonadal dysgenesis. Her adrenal functions were normal. Detailed gonadal and adrenal function tests and clinically significant laboratory test results are presented in Supplementary Table 1. She had high serum creatine kinase concentrations and severe diffuse myopathy diagnosed by electromyography. She had operations for omphalocele in newborn period and gonadectomized at $4^{2/12}$ years old. Histopathology of gonadectomy material revealed the only few clusters of Leydig cells and peripherally located Müllerian-like tubular structures in a loose connective tissue containing vessels and peripheral nerve bundles. At her last visit, she was $9^{10/12}$ years of age, weighted 19.5 kg (<3%), was 112.6 cm tall (<3%). Her span was 7.9 cm less than her height (<−2 SDS) and her upper/lower ratio was 0.96 (between −1 and 0 SDS). Her bone age was 5 years. Her serum IGF1, IGFBP3 concentrations and growth hormone stimulation tests were normal. She had two healthy siblings and one sister who was deceased at prenatal 7th month for an unknown reason. Two more relative couples in the family were reported to be infertile and could not have children following several years of marriage. They were unavailable for further investigation. One 37-year-old paternal female cousin did not develop any secondary sexual characteristics, did not have menstrual bleedings and never married. Her final height was around 142 cm. Facial gestalt of her was not similar to that of Patient 2. She had normal mental and motor functions. She was unavailable for clinical evaluation, karyotype or molecular analysis. One another relative in the family described as 'aunt' never developed secondary sexual characteristics, did not have menstrual bleedings and never married. Her final height was around 140–145 cm. She highly resembled Patient 2 and died at 60 years of age. She was unavailable for further investigation.

Family 3

$12^{8/12}$ years old female (Patient 3) was referred to our clinic for 46, XY gonadal dysgenesis. She was born to first-degree cousin parents at term with 2800 g birth weight (Fig. 1A). Her 38-year-old, 150.1 cm mother and 39-year-old, 175.5 cm father were well in general health. She had several common dysmorphic features and multisystem disorders similar to Patient 1 and Patient 2 noticed in 6.5 years of clinical follow-up (Fig. 1B and Table 1). Her karyotype was 46, XY with complete female external genitalia. Her hormonal evaluation was compatible with complete gonadal dysgenesis. Her adrenal functions were normal except some low/normal concentrations of adrenal sex steroids. Detailed gonadal and adrenal function tests and clinically significant laboratory test results are presented in Supplementary Table 1. She had high serum creatine kinase concentrations and severe diffuse myopathy diagnosed by electromyography. She was operated for developmental hip dysplasia at 3 years of age. There was no any gonad seen in laparoscopy at $13^{8/12}$ years old. Estrogen replacement was commenced at 14 years of age. Breast development Tanner stage 2 was attained at 14.5 years, pubic hair Tanner stage 2 was at 17.5 years and menarche was at 18 years. Her height SDS was between −2.5 and −3 SDS before estradiol therapy possibly due to significantly delayed bone age. At her last visit, she was $19^{2/12}$ years of age, weighted 48.4 kg (3-10%), was at a final height of 161 cm tall (25–50%). Her menstrual periods were regular under estrogen + progesterone replacement. She had sparse pubic hair but no axillary hair. Two more relatives in the family were reported to be infertile. They did not have secondary sexual characteristics. They married but could not have any children. They were unavailable for further investigation.

Family 4

A 5.5-month-old female (Patient 4) was referred to our clinic for 46, XY gonadal dysgenesis. She was born to first-degree cousin parents at term with 1900 g birth weight (Fig. 1A). Her 25-year-old, 160 cm mother and 34-year-old, 175 cm father were well in general health. She had several common dysmorphic features and multisystem disorders similar to Patients 1, 2 and 3 noticed in 1-year clinical follow-up (Fig. 1B and Table 1). Her karyotype was 46, XY with female external genitalia. Her hormonal evaluation was compatible with complete gonadal dysgenesis. Her adrenal functions were normal except some low/normal concentrations of adrenal sex steroids. She had high serum creatine kinase concentrations. Detailed gonadal and adrenal function tests and clinically significant laboratory test results are presented in Supplementary Table 1. She had operations for pyloric stenosis and omphalocele in the newborn period. She was gonadectomized at $1^{2/12}$ years old. Histopathology of gonadectomy material revealed no Leydig cells but peripherally located Müllerian-like tubular structures in a loose connective tissue containing vessels and peripheral nerve bundles. At her last visit, she was 1 years of age, weighted 6.25 kg (<3%), was 67 cm tall (<3%) and had a 40.6 cm head circumference (<3%). Two more relative couples in the family were reported to be infertile and could not have children following several years of marriages. They were unavailable for further investigation.

Molecular characteristics

WES was carried out for Patient 1 and Patient 2 due to the similarity in phenotypic and clinical characteristics. Variants were subjected to filtering as shown in Supplementary Table 2. The variants were selected by the following strategy: (i) homozygous variants due to consanguinity; (ii) variants with a minor allele frequency less than 0.01; (iii) variants in the coding sequence, splice variants, indels or duplications and nonsynonymous changes; (iv) variants with a coverage of at least 20 reads; (v) variants not recorded as benign in ClinVar database; (vi) selecting pathogenic or disease-causing variants by all base conservation scores and functional prediction tools (SIFT, Polyphen, Mutation Taster) (12-14) (dbSNP, http://www.ncbi.nlm.nih.gov/SNP/, release 85; Exome Aggregation Consortium [ExAC], accessed March 2017). Finally, the candidate variants in an only common gene (chr14:35568586A>G and chr14:35560340A>G in *PPP2R3C*) were investigated for segregation with disease in the families 1 and 2 by Sanger sequencing. Both variants were shown homozygous in patients and heterozygous in parents. We have evaluated the WES data of Patient 1 and 2 for all individual and shared homozygous, heterozygous and hemizygous variants of known testicular dysgenesis genes (*SRY*, *SOX9*, *WT1*, *NR5A1*, *SOX8*, *GATA4*, *DHH*, *FGF9*, *NR0B1*, *FOG2*, *MAP3K1*) as well as pathogenic or likely pathogenic variants in the other genes. None of the individual or shared variants were associated with pathogenicity. Moreover, we have also evaluated all other *PPP2R3C* variants in WES data of Patients 1 and 2 for any other potentially pathogenic variants and could not find any other variant that can be associated with the phenotype.

We subsequently identified homozygous variants in *PPP2R3C* in Patient 3 (c.308T>C; p.Leu103Pro) and Patient 4 (c.1049T>C; p.Phe350Ser) with a background of syndromic 46, XY DSD with similar phenotypic and clinical features using Sanger sequencing (Fig. 2A). In all cases, patients were homozygous for the change and parents were heterozygous. The c.1049T>C (p.F350S) variant seen in Patient 2 (family 2) was also identified in Patient 4 (family 4). Although there was no known relationship between these families, both families originated from the same city.

The variants identified in our patients were found neither in 200 ethnically matched in-house Turkish exomes and the Turkish whole-exome database nor in 20 in-house exomes from other Turkish 46, XY DSD patients. None of the variants were seen in either GnomAD, ExAC, 1000 Genomes, 6500ESP or the Turkish in-house databases. PolyPhen-2 predicts c.578 T>C (p.Leu193Ser), c.1049 T>C (p.Phe350Ser) and c.308T>C (p.Leu103Pro) as probably damaging, with scores of 0.985, 0.997 and 0.914 respectively. SIFT predicts all three variants as deleterious with scores of 0. Mutation Taster predicts all three variants to be disease causing. The PhyloP and PhastCons scores which are 4.719 and 1 for c.578T>C; 5.201 and 1 for 1049T>C; 5.139 and 1 for c.308T>C mutations show that these mutated regions are slowly evolving and conserved among species (Fig. 2B).

No detectable changes were identified in *PPP2R3C* mRNA expression levels derived from peripheral blood between the patients and healthy controls ($P=0.28$) (Fig. 2C). This shows that the reported missense variants do not significantly alter the expression of the gene but the function. While *PPP2R3C* mRNA is ubiquitously expressed in human tissues, highest expression is shown in the testis and in various datasets including GTeX and HPA datasets (https://www.proteinatlas.org/ENSG00000092020-PPP2R3C/tissue).

For protein modeling, among the five strongest 3D models created by LOMET server with highest confidence score are selected and used for analysis (Fig. 2D). The confidential score for wild and mutants in the helical structure is nine, and their predicted solvent accessibility is zero, implying that all were fully buried residues (Fig. 2E). The created models did not show critical differences between the alpha structures. Our I-Tasser models predicted *p*Ser350 alteration of the nonpolar residue phenylalanine to the hydroxyl group residue serine in the EF-hand domain would alter the tertiary structure of calcium-binding site. The EF-hand is a helix-loop-helix calcium-binding motif in which two helices pack together at and are separated by a loop region where calcium actually binds. That novel coding variant may be important in protein spatial interactions while presenting enzymatic activities.

PPP2R3C, SOX9 and SOX9-Phospho protein expression in normal fetal and adult testicular tissue and in the gonads from the patients with homozygous *PPP2R3C* variants

The gonadectomy materials from Patient 2 (at $4^{2/12}$ years old) and Patient 4 (at $1^{2/12}$ years old) were evaluated for histopathology and for the expression of PPP2R3C, SOX9 and SOX-Phosho proteins (Fig. 3A1–5 and 3B1–5). The control tissues were selected from a normal fetal testis obtained from an abortion at 18–19 weeks of gestation (Fig. 3C1–5) and a normal adult testis obtained from a 82-year-old man operated for prostate cancer (Fig. 3D1–5). H&E staining revealed normal Leydig cells and seminiferous tubular structures in the control fetal (Fig. 3C1) and adult testis (Fig. 3D1), and the gonadal biopsy of Patient 2 revealed only few clusters of Leydig cells and peripherally located Müllerian-like tubular structures in a loose connective tissue containing vessels and peripheral nerve bundles (Fig. 3A1 and A2). The gonadal biopsy of Patient 4 revealed no Leydig cells but peripherally located Müllerian-like tubular structures in a loose connective tissue containing vessels and peripheral nerve bundles (Fig. 3B1 and B2). Inhibin immunohistochemical staining indicates Leydig cells (Fig. 3A2, C2 and D2). The gonad tissue of Patient 4 was negative for inhibin immunostaining due to the absence of Leydig cells (Fig. 3B2). PPP2R3C is ubiquitously expressed in human testis from fetal period to the adulthood (Fig. 3C3 and D3). PPP2R3C expression was seen in Patient 2 and in Patient 4 similar to control tissues (Fig. 3A3 and B3). The Müllerian-like tubules from Patient 2, Patient 4 and the seminiferous tubules of the control fetal and adult testis sections were positive for SOX9 protein immunostaining (Fig. 3A4, B4, C4 and D4). SOX9 is a downstream canonical target of PP2A. SRY-mediated SOX9 upregulation in the early gonad is crucial for testis development. SOX9 needs to be phosphorylated to SOX9-Phospho to be activated to induce downstream pathways for testicular development. The variants in *PPP2R3C* are predicted to upregulate the catalytic function of PP2A, subsequently increasing the dephosphorylation of SOX9-Phospho. Disruption in testis development due to impaired SOX9-Phospho signaling was supported by the analysis of SOX9-Phospho in the gonad tissues from Patient 2 and Patient 4 with homozygous *PPP2R3C* variants, which showed no expression of SOX9-Phospho

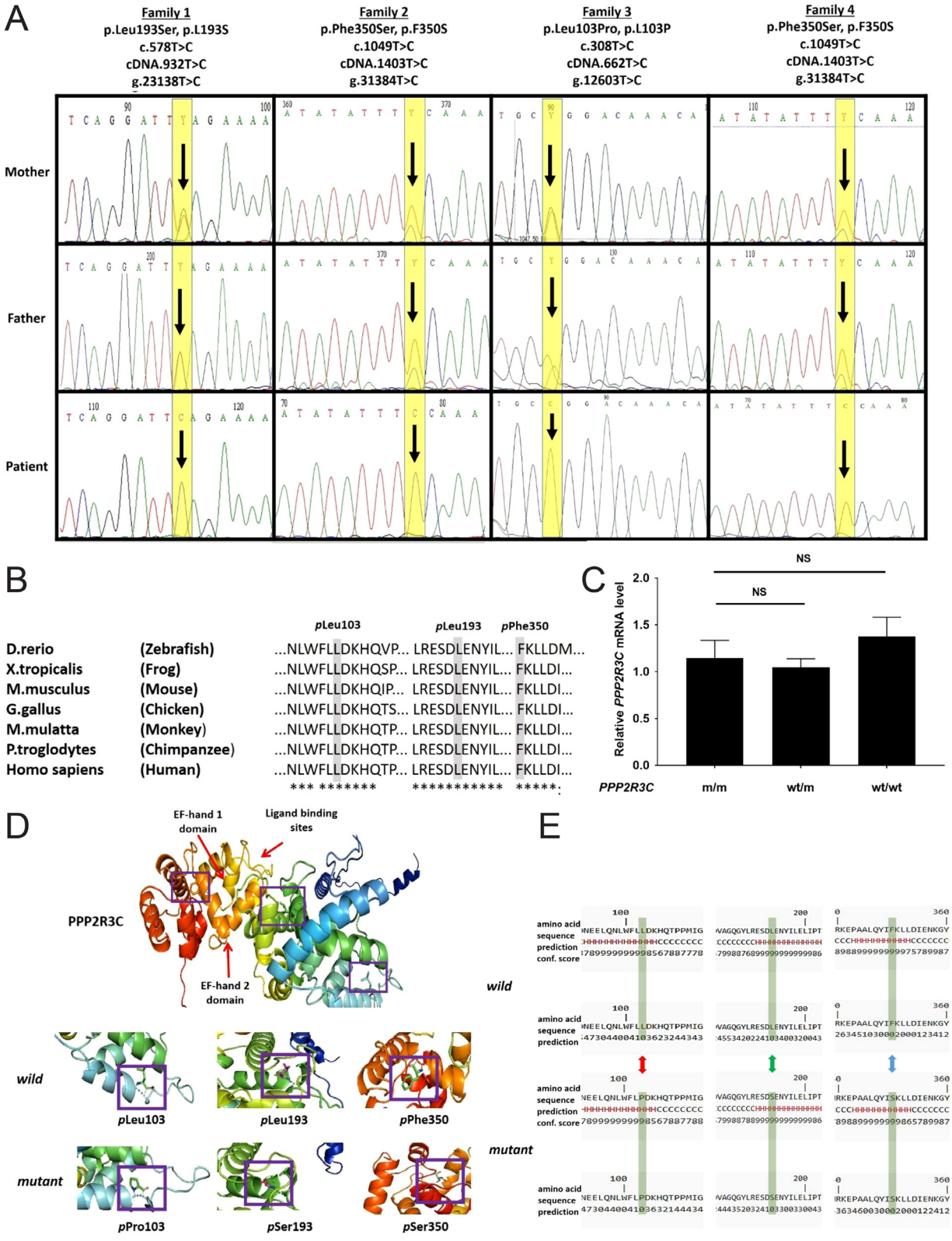

Figure 2

Molecular analysis of patients with the *PPP2R3C* variants. (A) Electropherogram showing the homozygous *PPP2R3C* variants (the black arrows and yellow boxes indicates the nucleotide peak of interest) in probands and respective heterozygous variants in

European Journal of Endocrinology

(Fig. 3A5 and 3B5) compared to normal expression in fetal and adult testis tissues (Fig. 3C5 and 3D5).

Reproductive functions of individuals with heterozygous *PPP2R3C* variants

The autosomal recessive mode of inheritance of the syndrome and the existence of infertile cases in the affected families including the parents of Patient 1, prompted us to investigate the reproductive functions of the parents who were genotype-proven carriers of deleterious *PPP2R3C* variants (Table 2). Semen analyses was performed in all fathers except the father of Patient 2. All three fathers (infertile father of Patient 1 and apparently fertile fathers of patients 3 and 4) were found to have teratozoospermia with severe head, acrosomal and nuclear abnormalities (Fig. 4 and Table 2). The mother of Patient 1 reported oligomenorrhea and hypomenorrhea with no abnormality in pelvic ultrasonography; mother of Patient 3 had menopause at 44 years of age. Other two mothers had regular menstrual periods.

Evaluation of B lymphocyte viability, proliferation rate and apoptosis

Since B lymphocytes of *PPP2R3C*-null mice showed impaired viability and proliferation and increased apoptosis (7), analyses were focused on $CD19^+$ B lymphocytes obtained from patients with homozygous *PPP2R3C* variants (Patients 1, 2, 3). Annexin V/PI staining revealed that, in terms of viability, there was no significant difference between 0 and 24th hours among patients; however, viable cell rate was significantly decreased between 24 and 48 h (Fig. 5B); early apoptosis rate was increased between these two time points (Fig. 5C). Late apoptosis was increased significantly at 48 h (Fig. 5C). Alterations of necrosis rates were not significant in three time points (Fig. 5D). When compared with age-matched healthy individuals ($n=6$; three females and three males), patients' viable cell population was lower on 48th hour (Fig. 5F), and this decrease was accompanied by increased early and late apoptotic cell ratios (Fig. 5G and H). Altogether, these data may suggest that patients' $CD19^+$ B lymphocytes are more susceptible to apoptosis compared to healthy controls. Moreover, DNA content analysis revealed that no difference between 0, 24th and 48th hours and G_1/G_0 phase was significantly decreased compared to hour 0 supporting a decreased proliferation of B lymphocytes (Fig. 5J and K).

Discussion

Here, we describe a novel autosomal recessive 46, XY gonadal dysgenesis syndrome due to the variants in *PPP2R3C* gene in four girls from four unrelated families. Besides complete testicular dysgenesis, a number of extra gonadal anomalies, including typical facial gestalt, low birth weight, myopathy, rod and cone dystrophy, anal atresia, omphalocele, sensorineural hearing loss, dry and scaly skin, skeletal abnormalities, renal agenesis and neuromotor delay characterize this syndrome. Furthermore, our findings show that heterozygous defects of this gene are associated with impaired spermatogenesis and male infertility.

their parents. (B) Partial alignment of PPP2R3C protein sequences, generated by Clustal Omega (https://www.ebi.ac.uk/Tools/msa/clustalo/), showing conservation of leucine (Leu;L) at position 103, leucine (Leu;L) at position 193 and phenylalanine (Phe;F) at position at 350 highlighted in gray, with numbering relative to human sequence. These amino acids are highly conserved among ortholog proteins. (C) Levels of *PPP2R3C* mRNA were quantified by RT-qPCR and were unchanged between control (wt/wt), parents (wt/m) and patients (m/m). The column and whisker graph represents the mean and standard errors of mean (S.E.M.) of the measurements. NS, not significant. (D) Schematic domains and ligand-binding sites of PPP2R3C (UniprotKB: Q969Q6) are illustrated. These include a EF-hand 1 (residues 273-308), EF-hand 2 (341-376) domain and calcium-binding site (286-297). The location of the domains is marked by the red arrows. Locations of *p*Leu103, *p*Leu193 and *p*Phe350 of wild-type PPP2R3C and *p*Pro103, *p*Ser193 and *p*Ser350 identified in our patients are presented in magnified frame for viewing at higher quality. The models are visualized by PyMol, with rainbow painting starting from dark blue at 'N terminal' and ending red at 'C terminal'. Elements of residues are painted in stick format and view zoomed to 20 Å below for each model. (E) Secondary structure and the solvent accessibility scores of the investigated wild type and mutation sites are presented in I-Tasser simulated models. Predicted secondary structure is scored from zero to nine; the higher the score, the more confident is the prediction. The predicted secondary structure suggests that this protein is an alpha-beta protein. 'H' and 'C' indicate helix and coil, respectively. The predicted solvent accessibility at the bottom is presented in ten levels, from buried (zero) to higher exposed (eight). *p*Leu103 residues are pointed with red, *p*Ser193 with green and *p*Ser350 with blue arrows.

Reversible protein phosphorylation is one of the most common posttranslational modifications of proteins and represents an essential mechanism of signal transduction in cell. A broad range of intracellular processes is regulated by reversible phosphorylation–dephosphorylation of proteins depending on a fine balance between the actions of protein kinases and protein phosphatases, respectively. Protein phosphatase 2A (PP2A) is the major Ser/Thr phosphatase in most cell types. The PP2A is a heterotrimeric holoenzyme consisting of a scaffolding A, catalytic C and a regulatory B subunits (5, 15) (Supplementary Fig. 2). The regulatory subunits are the

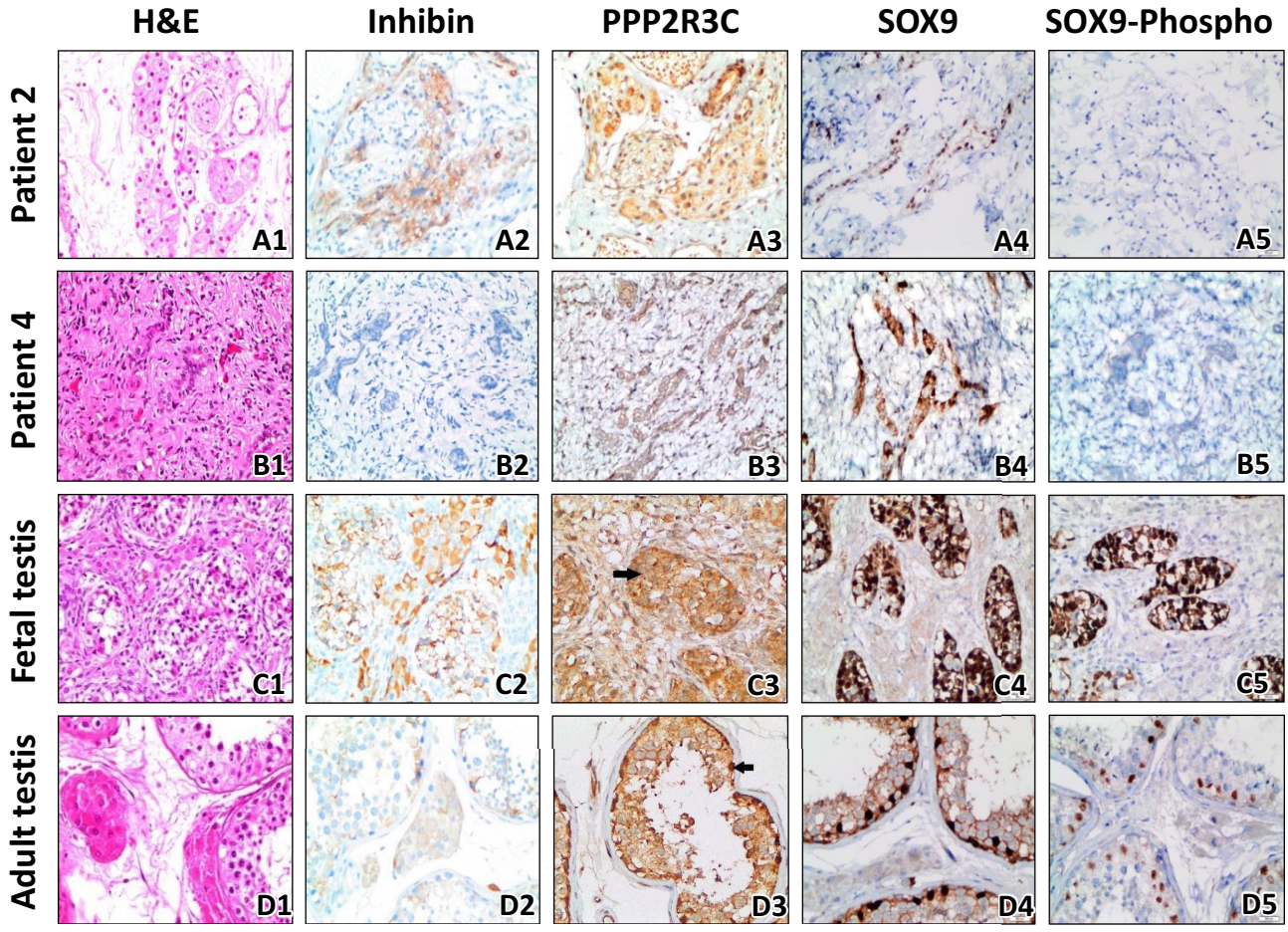

Figure 3

Overview of histology and, PPP2R3C, SOX9 and SOX9-Phospho protein expressions in the dysgenetic gonads from Patient 2, Patient 4, and the developing normal fetal testis and adult testis tissues. The representative images of the gonadal tissues of Patient 2 and Patient 4 are shown in the upper 1st and the 2nd panels (A1–5, B1–5). The control tissues were selected from a normal fetal testis (C1–5) and a normal adult testis (D1–5). H&E staining revealed normal Leydig cells and seminiferous tubular structures in the control fetal (C1) and adult testis (D1). The gonadal tissue of Patient 2 revealed only few clusters of Leydig cells and peripherally located Müllerian-like tubular structures in a loose connective tissue containing vessels and peripheral nerve bundles (A1, A2). The gonadal biopsy of Patient 2 revealed no Leydig cells but peripherally located Müllerian-like tubular structures in a loose connective tissue containing vessels and peripheral nerve bundles (B1, B2). Inhibin immunohistochemical staining indicates Leydig cells (A2, C2, D2). The gonad tissue of Patient 4 was negative for inhibin immunostaining due to the absence of Leydig cells (B2). PPP2R3C expression was seen in Patients 2 and 4 similar to control tissues (A3, B3, C3, D3). PPP2R3C immunoreactivity in Sertoli cells of seminiferous tubules of control testis tissues is indicated by black arrows in C3, D3. Note that the Müllerian-like tubules were positive for SOX9 (A4, B4), but are negative for SOX9-Phospho protein expression (A5, B5) in the Patient 2 and Patient 4 with homozygous *PPP2R3C* variants. However, the seminiferous tubules of the control testis sections were positive for both SOX9 (C4, D4) and SOX9-Phospho (C5, D5) immunostaining (images are at ×40 magnification).

Table 2 The gonadal and adrenal function test results of heterozygous pathogenic *PPP2R3C* mutation carriers.

Feature	Patient 1		Patient 2		Patient 3		Patient 4	
	Mother (36 years old)	Father (38 years old)	Mother (34 years old)	Father (38 years old)	Mother (45 years old)	Father (46 years old)	Mother (26 years old)	Father (35 years old)
FSH (mIU/mL) (normal range)	2.44 (1.79–5.12)	5.68 (1.2–19.2)	5.06 (3.85–8.78)	5.01 (1.27–19.26)	43.15 (1.27–19.26)	5.61 (1.27–19.2)	8.94 (3.85–8.78)	2.7 (1.27–19.26)
LH (mIU/mL) (normal range)	3.02 (1–11)	4.09 (1.7–8.6)	14.71 (2.4–12.6)	7.65 (1.7–8.6)	12.76 (2.4–12.6)	8.16 (1.87–8.6)	5.14 (2.4–12.6)	3.58 (1.7–8.6)
Testosterone (ng/mL)	–	2.2 (2.4–9.5)	–	4.77 (2.4–9.5)	–	3.11 (2.4–9.5)	–	3.84 (2.4–9.5)
Estradiol (ng/mL)	107.2 (22–341)	–	150 (12.4–233)	–	27.55	–	52.81 (12.4–233)	–
Anti-Mullerian hormone (ng/mL) (normal range)	0.59 (0–7.3)	10.95 (0.7–16)	3.66 (0.36–10.7)	3.03 (0.7–19)	0.16 (1.02–14.63)	3.29 (0.7–19)	3.61 (1.02–14.63)	9.23 (0.7–19)
DHEAS (ng/mL) (normal range)	163 (35–430)	323 (80–560)	259 (35–430)	82.5 (80–560)	40.7 (35–430)	124.6 (80–560)	110 (35–430)	203.5 (80–560)
Androstenedione (ng/mL) (normal range)	1.06 (0.3–2)	1.11 (0.6–3.1)	1.78 (0.3–3.3)	0.91 (0.6–3.1)	0.28 (0.2–0.75)	<0.3 (0.6–3.1)	0.77 (0.3–2)	0.54 (0.4–1.9)
Semen analysis	–	Teratozoospermia	–	NA	–	Teratozoospermia	–	Teratozoospermia
Volume (mL) (>2)		3		NA		2.1		2.8
Concentration (million/mL) (>15)		38		NA		32		38
Motility (%) (>40)		48		NA		44		72
Normal morphology (%) (>4)		1		NA		2		4
Abnormal morphology (%)		Severe head (53%), severe acrosomal (25%), severe nuclear (26%) and other minor anomalies		NA		Mild head (5%), severe acrosomal (15%), severe nuclear (14%) and other minor anomalies		Mild head (10%), severe acrosomal (27%), severe nuclear (27%), double tail (11%) and other minor anomalies

DHEAS, dehydroepiandrosterone sulfate; FSH, follicle-stimulating hormone; LH, luteinizing hormone.

main determinants of target tissue, substrate specificity and the function of PP2A. There are 16 B-type subunits, which suggest a broad range of PP2A function in diverse cellular processes and dysfunction of any regulatory subunit may be associated with a different clinical presentation. *PPP2R3C* encodes B″gamma regulatory subunit of PP2A (5, 15) (Supplementary Fig. 2).

PPP2R3C shows the highest mRNA and protein expression in human testicular structures, secondly in the lymphocytes (https://www.proteinatlas.org/ENSG00000092020-PPP2R3C/tissue). The conditional and targeted knockout mice model of *PPP2R3C* showed decreased survival and increased apoptosis of B lymphocytes which is the only *in vivo* function of PPP2R3C reported so far. However, since PPP2R3C$^{-/-}$ B lymphocytes showed a normal proliferative response to lipopolysaccharide and other antigenic stimuli in mice, immunodeficiency was not seen (6, 7). Our results on CD19^{+} B lymphocytes obtained from the patients with homozygous *PPP2R3C* variants revealed a decreased viability and proliferation rate and an increased early and late apoptosis of CD19^{+} B lymphocytes. These results are in line with the data from lymphoid tissue-targeted *PPP2R3C*-null mice (6, 7). Our patients also did not show any clinical immunodeficiency symptoms or increased tendency to infections. Serum immunoglobulin concentrations and lymphocyte counts were normal in all patients. Instead, 46, XY complete gonadal dysgenesis was the main symptom of referral in all four patients in our cohort. Since it was a lymphoid tissue-targeted *PPP2R3C*-knockout mice, the gonadal phenotype would be expected as uninformative. Nevertheless, there are a number of evidence supporting the pivotal role of PP2A and its subunits in testicular development and spermatogenesis.

In vivo studies using mutants of *Saccharomyces cerevisiae* and *Drosophila* showed that the B regulatory subunit of PP2A is required for completion of anaphase and microtubule organization in cell cycle (16, 17). Kitagawa *et al*. were the first to describe the remarkable expression of small-sized mRNAs for catalytic subunits of PP2A (PP-2Aβ) (by which they were possibly meaning the subtypes of regulatory B subunits) in testis and testicular germ cells of rat including spermatogonia, primary spermatocytes, secondary spermatocytes and spermatids. They have suggested that protein phosphatases may play a role in of in cell-cycle regulation during the meiosis of spermatogonia (18). In 1993, Hatano *et al*. showed that B regulatory subunit of PP2A (BRβ) was specifically expressed in rat brain and testis. In rat testis, BRβ expression is increased after 40th days and is involved in the spermatid elongation through the action of tau protein (19). Tau protein is a microtubule-associated protein located in both neuronal axons and the manchett of the elongated spermatid (20). Tau protein has been reported to be phosphorylated at serine/threonine residues (21), dephosphorylated by PP2A *in vitro* and is probably involved in the microtubule polymerization (22). Hatano *et al*. have shown co-expression of tau and BRβ in the elongated spermatids and suggested tau as one of the target substrates of PP2A (19). van den Ham *et al*. investigated the expression of scaffolding subunit A of PP2A (PP2A-A) during testicular development of rats of various ages from 16 days postcoitum (pc) to adulthood (23). Their protein expression data from *in situ* hybridization, immunohistochemistry and Western blot analyses revealed that both spermatogonia and Sertoli cells express PP2A-A during their proliferative period at various stages of testicular development from fetal 19 days pc to 15 days postpartum. This study shows that PP2A may play an important role in the testicular development and spermatogenesis (23). In line with these data, we have demonstrated the expression of PPP2R3C protein in the normal human testis from the fetus at the 18th week of gestation to the adulthood at 82 years old. Furthermore, we have shown teratozoospermia in the fathers of our patients who were heterozygous for *PPP2R3C* defect, although two of them had no clinically apparent infertility

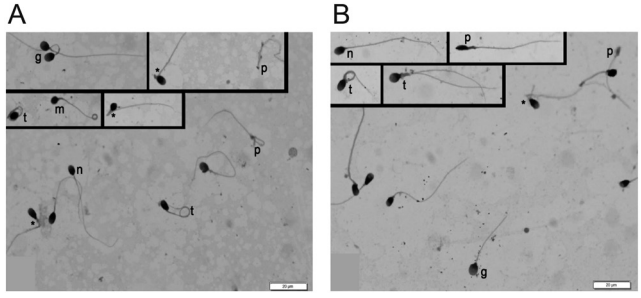

Figure 4

Representative light micrographs of semen smears from the fathers of Patient 3 (A) and Patient 4 (B). *, midpiece defect; m, mixed defect (head and tail); n, normal spermatozoa; g, globozoospermatozoa; p, pinhead spermatozoa; t, tail defect (dag or double tail). Diff-Quick staining. The father of Patient 3 showed a few number of normal spermatozoa. Head defects with globozoospermatozoa and pinhead were observed in both patients. Moreover, spermatozoa with mixed defects (head, midpiece and tail) were present. There were severe tail defects in both patients. However, tail defects with double tail were more prominent in the father of Patient 4.

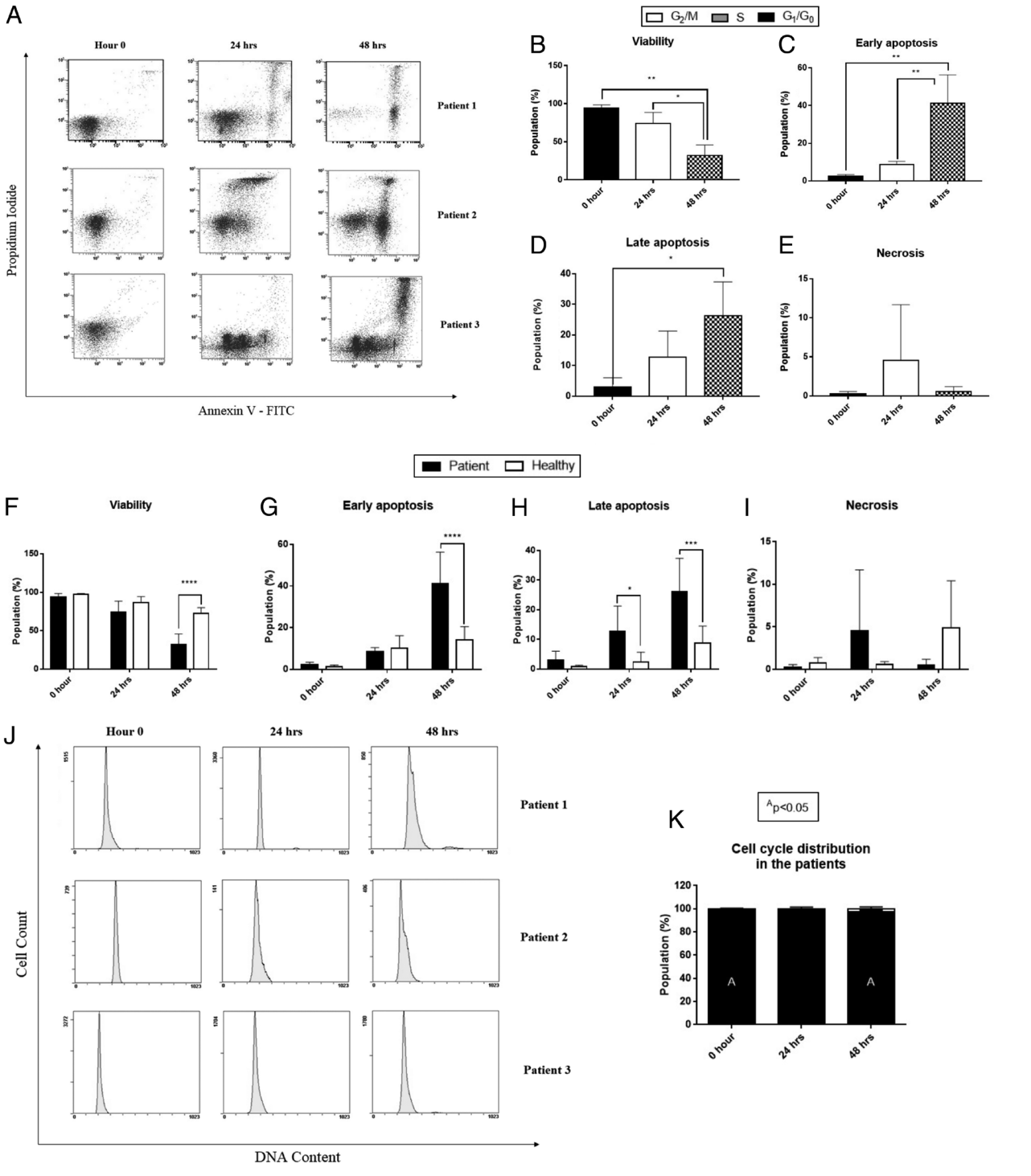

Figure 5

Evaluation of CD19⁺ B lymphocytes for viability, apoptosis and cell-cycle characteristics in patients with homozygous *PPP2R3C* variants. (A) Dot plots of three patients' Annexin V/PI staining. (B, C, D and E) The viability, early apoptosis, late apoptosis and necrosis ratios of B lymphocytes were compared at 0, 24 and 48 h after blood sampling from patients with PPP2R3C variants. (F, G, H and I) Comparison between patients' and control samples' for viability, early apoptosis, late apoptosis and necrosis ratios of B lymphocytes. (J) Histogram plots of three patients' DNA content analysis. (K) Statistical analysis of cell-cycle distribution (G_2/M, S, G_1/G_0) between three time points. $P < 0.05$ is considered significant (*$P = 0.01$; ***$P < 0.001$; ****$P < 0.0001$).

problem. Taken together, 46, XY complete gonadal dysgenesis described in four patients with homozygous *PPP2R3C* variants and, teratozoospermia and infertility in the heterozygous carriers of deleterious *PPP2R3C* variants in this study provides the first *in vivo* human evidence on the key role of PPP2R3C protein in the testicular development and identifies it as a critical intracellular signaling molecule involved in spermatogenesis.

Main syndromic facial features in our patients are related to ear and nose cartilage which suggests that chondrogenesis is impaired in addition to testicular dysgenesis. Sex-determining region Y (SRY)-box 9 (SOX9) has fundamental functions in several developmental processes, including testis development (24, 25), maintenance and the integrity of Sertoli cells in adult testis (26) and is essential for early chondrogenesis (27). Campomelic dysplasia (OMIM #114290) is a well-known disorder of chondrogenesis associated with 46, XY sex reversal due to *SOX9* mutations. Duplications and deletions of enhancers upstream of *SOX9* have recently been shown to cause sex reversal in 46, XX and 46, XY individuals respectively (28, 29). SOX9 is also subjected to multiple posttranscriptional modifications in testicular development and chondrogenesis. Phosphorylation by protein kinase A (PKA) enhances DNA-binding affinity of SOX9 and leads to its translocation into the nucleus in testis cells (30). Interestingly, this same event is also required for parathyroid hormone-related peptide (PTHrP)-mediated regulation of chondrocyte maturation (31). PP2A plays a role in the regulation of the PKA signaling pathway and that the phosphorylation level of CREB is influenced by the activity of both enzymes during *in vitro* chondrogenesis. The chondrogenesis-promoting effect of PKA via SOX9 (at Ser 211) and CREB phosphorylation is counterbalanced by the activity of protein phosphatase 2A (PP2A), a negative regulator of chondrogenesis (32). Main targets of SOX9 transcription factor are Testatin, Collagen type IV and Collagen type IX (33). The phosphorylation and, consequently, the activation of SOX9 is regulated by protein kinase A and increased PP2A activity has been shown to be responsible for decreased phosphorylation of SOX9 (34). We suggest that the variants in *PPP2R3C* upregulate the catalytic function of PP2A and increase the dephosphorylation of SOX9-Phospho protein. The decreased SOX9-Phospho protein expression in the dysgenetic gonads of the patients with homozygous *PPP2R3C* variants presents a solid base of evidence for impaired SOX9 signaling in the pathogenesis of gonadal dysgenesis in this condition. Collectively, we suggest that PPP2R3C is a key player by which SOX9 regulates testis development in humans, and identified *PPP2R3C* variants as a significant cause of 46, XY testicular dysgenesis.

From the biosynthesis of testicular and adrenal androgen point of view, the equilibrium between the phosphorylation and dephosphorylation of the proteins are important. Recent studies identified the mitogen-activated protein kinase 14 (MAPK14, p38α) enhancing 17,20 lyase activity by phosphorylation (35, 36), while PP2A was shown to dephosphorylate CYP17A1 and diminish lyase activity and androgen synthesis in the testis and adrenals (37). Although there were no clinically significant impairment in the androgen production either in heterozygous males or in females, there were noticeable low-normal values in adrenal and gonadal androgen concentrations. This effect may not be significant because of the heterozygosity of genetic defect or compensation of the defect by some other intact pathways of androgen biosynthesis. In homozygous patients, the low adrenal androgen concentrations were more significant especially in androstenedione levels, which is the main product of 17,20 lyase activity. The absence of axillary hair and sparse pubic hair attained at 17.5 years old in the eldest patient in this cohort also suggests impaired adrenal androgen biosynthesis in this syndrome.

Based on the above-mentioned data, serine/threonine phosphorylation of the canonical downstream signaling proteins including SOX9, MAPK14, Tau and CYP17A1 favor normal testicular development, spermatogenesis and androgen biosynthesis. Therefore, the phenotype of testicular dysgenesis, abnormal spermatogenesis and decreased androgen synthesis in the patients with *PPP2R3C* variants are associated with increased dephosphorylation. *PPP2R3C* variants upregulate the catalytic activity of PP2A, subsequently dephoshorylation process of the related proteins dominates, thus resulting in a multi-hit mechanism against male sex development and fertility (Supplementary Fig. 3).

The *PPP2R3C* variants identified in our patients were not reported on large population databases including gnomAD and show a significant conservation in the general population and among multiple orthologs. GnomAD reports no coding homozygous *PPP2R3C* variants in the healthy population. However, *PPP2R3C* has a probability of loss-of-function intolerance (pLI) score of 0.0 in population metrics based on gnomAD, which indicates that heterozygous loss-of-function mutations are likely to be benign (38). Eight heterozygous carriers of pathogenic *PPP2R3C* variants have been evaluated in our study who were apparently healthy parents of our patients. These individuals did not have any phenotypical features

or any clinically significant systemic involvement unlike the patients with homozygous *PPP2R3C* mutations. They had noticeable but clinically insignificant low-normal values in adrenal and gonadal androgen concentrations. Moreover, we have identified normal sperm counts and sperm motility but abnormal sperm morphology in three heterozygous fathers. Two of them had no history of infertility. Therefore, although the heterozygosity of *PPP2R3C* variants is associated with impaired spermatogenesis, the general clinical presentation of heterozygosity of *PPP2R3C* variants may likely be benign. Selective pharmacologic PP2A inhibitors, such as okadaic acid was shown to promote fertility by increasing sperm motility, velocity and lateral head amplitude (39, 40) which is in line with the proposed pathogenesis. Thus, our findings about the role PPP2R3C in spermatogenesis in humans have also implications for novel therapeutic targets of human infertility.

Brosnan *et al*. described two sisters with syndromic 46, XY complete gonadal dysgenesis and multiple anomalies in ectodermal and mesodermal structures in 1980 (41). Although the authors reported that parents were nonconsanguineous and no molecular study was done at that time, those two girls had the same clinical features with that of our cohort including common facial gestalt with multisystem involvements, particularly affecting skin, muscles and gonads. Therefore, we think that these two sisters had the same syndrome as described in the present study. We would like to propose the name Myo-Ectoderma-Gonadal Dysgenesis (MEGD) for this novel syndrome.

Rare human phenotypes related to genetic defects in the subunits of PP2A were described very recently. Heterozygous *de novo* missense mutations in PP2A regulatory subunit B family genes, *PPP2R5B*, *PPP2R5C* and *PPP2R5D*, have recently been described in individuals with overgrowth and intellectual disability (42). *De novo* mutations affecting the catalytic Cα subunit of PP2A (*PPP2CA*) were identified to cause a syndromic intellectual disability and developmental delay (43). However, no homozygous mutations was identified in those conditions. None of these patients had a consistent facial gestalt nor had a reportable gonadal abnormality. Moreover, we have evaluated the WES data of Patient 1 and 2 for all individual and shared homozygous, heterozygous and hemizygous variants of *PPP2R5B*, *PPP2R5C*, *PPP2R5D* and *PPP2CA* genes and could not find any other variant that can be associated with the phenotype. This also supports that PPP2R3C is a highly specific B subunit determining the pivotal function of related PP2A complex in testis, male germ cells, muscles, skin and various ectodermal tissues.

In summary, we characterize a novel syndrome of 46, XY complete gonadal dysgenesis and a constellation of ectodermal, muscular and multisystem abnormalities. Our findings collectively identify PPP2R3C as an important factor for human development, especially a novel factor for testis development and spermatogenesis.

Supplementary data

This is linked to the online version of the paper at https://doi.org/10.1530/EJE-19-0067.

Declaration of interest

The authors declare that there is no conflict of interest that could be perceived as prejudicing the impartiality of this study.

Funding

This work has been supported by the Medical Research Council of Marmara University (Project Grant SAG-A-120418-0152, T G).

Author contribution statement

T G, G Y and B K designed the study. T G, S T, Z A and A B recruited and clinically characterized the patients. T G and G Y analyzed WES data. T G and G Y conducted Sanger sequencing and analysis of the results. S A, S G and B K conducted and analyzed quantitative real-time PCR. A A generated protein models of mutated PPP2R3C residues. E B and F S E conducted histopathology studies. I T, M K K and F E conducted sperm analysis and light microscopic studies. B A and G Y D conducted lymphocyte immunophenotyping and apoptosis assessments. T G, G Y, B K, F S E, F E, S T and A B prepared the draft manuscript. All authors contributed to the discussion of results, and edited and approved the final manuscript.

Acknowledgments

The authors thank Prof Uygar Halis Tazebay for useful discussions on the design of the study. They thank to Busra Kaya, Kubra Hacibeyoglu and Banu Buyukturgay for their technical assistance in Sanger sequencing and immunohistochemistry studies. They are deeply grateful to the patients and families without whom this study could not have been performed.

References

1 Del Valle I, Buonocore F, Duncan AJ, Lin L, Barenco M, Parnaik R, Shah S, Hubank M, Gerrelli D & Achermann JC. A genomic atlas of human adrenal and gonad development. *Wellcome Open Research* 2017 **2** 25. (https://doi.org/10.12688/wellcomeopenres.11253.2)

2 Lee PA, Nordenström A, Houk CP, Ahmed SF, Auchus R, Baratz A, Baratz Dalke K, Liao LM, Lin-Su K, Looijenga LHJ *et al*. Global disorders of sex development update since 2006: perceptions, approach and care. *Hormone Research in Paediatrics* 2016 **85** 158–180. (https://doi.org/10.1159/000442975)

3 Kremen J, Chan YM & Swartz JM. Recent findings on the genetics of disorders of sex development. *Current Opinion in Urology* 2017 **27** 1–6. (https://doi.org/10.1097/MOU.0000000000000353)

4 Kim JH, Kang E, Heo SH, Kim GH, Jang JH, Cho EH, Lee BH, Yoo HW & Choi JH. Diagnostic yield of targeted gene panel sequencing to identify the genetic etiology of disorders of sex development. *Molecular and Cellular Endocrinology* 2017 **444** 19–25. (https://doi.org/10.1016/j.mce.2017.01.037)

5 Reynhout S & Janssens V. Physiologic functions of PP2A: lessons from genetically modified mice. *Biochimica et Biophysica Acta: Molecular Cell Research* 2019 **1866** 31–50. (https://doi.org/10.1016/j.bbamcr.2018.07.010)

6 Xing Y, Igarashi H, Wang X & Sakaguchi N. Protein phosphatase subunit G5PR is needed for inhibition of B cell receptor-induced apoptosis. *Journal of Experimental Medicine* 2005 **202** 707–719. (https://doi.org/10.1084/jem.20050637)

7 Kitabatake M, Toda T, Kuwahara K, Igarashi H, Ohtsuji M, Tsurui H, Hirose S & Sakaguchi N. Transgenic overexpression of G5PR that is normally augmented in centrocytes impairs the enrichment of high-affinity antigen-specific B cells, increases peritoneal B-1a cells, and induces autoimmunity in aged female mice. *Journal of Immunology* 2012 **189** 1193–1201. (https://doi.org/10.4049/jimmunol.1102774)

8 Li H & Durbin R. Fast and accurate long-read alignment with Burrows-Wheeler transform. *Bioinformatics* 2010 **26** 589–595. (https://doi.org/10.1093/bioinformatics/btp698)

9 McKenna A, Hanna M, Banks E, Sivachenko A, Cibulskis K, Kernytsky A, Garimella K, Altshuler D, Gabriel S, Daly M *et al.* The Genome Analysis Toolkit: a MapReduce framework for analyzing next-generation DNA sequencing data. *Genome Research* 2010 **20** 1297–1303. (https://doi.org/10.1101/gr.107524.110)

10 Wang K, Li M, Hakonarson H & ANNOVAR. Functional annotation of genetic variants from high-throughput sequencing data. *Nucleic Acids Research* 2010 **38** e164.

11 1000 Genomes Project Consortium, Abecasis GR, Auton A, Brooks LD, DePristo MA, Durbin RM, Handsaker RE, Kang HM, Marth GT & McVean GA. An integrated map of genetic variation from 1092 human genomes. *Nature* 2012 **491** 56–65. (https://doi.org/10.1038/nature11632)

12 Sim NL, Kumar P, Hu J, Henikoff S, Schneider G & Ng PC. SIFT web server: predicting effects of amino acid substitutions on proteins. *Nucleic Acids Research* 2012 **40** W452–W457. (https://doi.org/10.1093/nar/gks539)

13 Adzhubei I, Jordan DM & Sunyaev SR. Predicting functional effect of human missense mutations using PolyPhen-2. *Current Protocols in Human Genetics* 2013 **Ch 7** Unit 7.20. (https://doi.org/10.1002/0471142905.hg0720s76)

14 Schwarz JM, Cooper DN, Schuelke M & Seelow D. MutationTaster2: mutation prediction for the deep-sequencing age. *Nature Methods* 2014 **11** 361–362. (https://doi.org/10.1038/nmeth.2890)

15 Moorhead GB, Trinkle-Mulcahy L & Ulke-Lemée A. Emerging roles of nuclear protein phosphatases. *Nature Reviews: Molecular Cell Biology* 2007 **8** 234–244. (https://doi.org/10.1038/nrm2126)

16 Healy AM, Zolnierowicz S, Stapleton AE, Goebl M, DePaoli-Roach AA & Pringle JR. CDC55, a Saccharomyces cerevisiae gene involved in cellular morphogenesis: identification, characterization, and homology to the B subunit of mammalian type 2A protein phosphatase. *Molecular and cellular Biology* 1991 **11** 5767–5780.

17 Wera S, Fernandez A, Lamb NJ, Turowski P, Hemmings-Mieszczak M, Mayer-Jaekel RE & Hemmings BA. Deregulation of translational control of the 65-kDa regulatory subunit (PR65 alpha) of protein phosphatase 2A leads to multinucleated cells. *Journal of Biological Chemistry* 1995 **270** 21374–21381. (https://doi.org/10.1074/jbc.270.36.21374)

18 Kitagawa Y, Sasaki K, Shima H, Shibuya M, Sugimura T & Nagao M. Protein phosphatases possibly involved in rat spermatogenesis. *Biochemical and Biophysical Research Communications* 1990 **171** 230–235. (https://doi.org/10.1016/0006-291X(90)91381-2)

19 Hatano Y, Shima H, Haneji T, Miura AB, Sugimura T & Nagao M. Expression of PP2A B regulatory subunit beta isotype in rat testis. *FEBS Letters* 1993 **324** 71–75. (https://doi.org/10.1016/0014-5793(93)81535-8)

20 Ashman JB, Hall ES, Eveleth J & Boekelheide K. Tau, the neuronal heat-stable microtubule-associated protein, is also present in the cross-linked microtubule network of the testicular spermatid manchette. *Biology of Reproduction* 1992 **46** 120–129. (https://doi.org/10.1095/biolreprod46.1.120)

21 Ishiguro K, Omori A, Sato K, Tomizawa K, Imahori K & Uchida T. A serine/threonine proline kinase activity is included in the Tau protein kinase fraction forming a paired helical filament epitope. *Neuroscience Letters* 1991 **128** 195–198. (https://doi.org/10.1016/0304-3940(91)90259-V)

22 Goedert M, Cohen ES, Jakes R & Cohen P. p42 MAP kinase phosphorylation sites in microtubule-associated protein tau are dephosphorylated by protein phosphatase 2A1. Implications for Alzheimer's disease. *FEBS Letters* 1992 **312** 95–99. (https://doi.org/10.1016/0014-5793(92)81418-L)

23 van den Ham R, van Dissel-Emiliani FM & van Pelt AM. Expression of the scaffolding subunit A of protein phosphatase 2A during rat testicular development. *Biology of Reproduction* 2003 **68** 1369–1375. (https://doi.org/10.1095/biolreprod.102.004853)

24 Barrionuevo F & Scherer G. SOX E genes: SOX9 and SOX8 in mammalian testis development. *International Journal of Biochemistry and Cell Biology* 2010 **42** 433–436. (https://doi.org/10.1016/j.biocel.2009.07.015)

25 Georg I, Barrionuevo F, Wiech T & Scherer G. Sox9 and Sox8 are required for basal lamina integrity of testis cords and for suppression of FOXL2 during embryonic testis development in mice. *Biology of Reproduction* 2012 **87** 99. (https://doi.org/10.1095/biolreprod.112.101907)

26 Barrionuevo FJ, Hurtado A, Kim GJ, Real FM, Bakkali M, Kopp JL, Sander M, Scherer G, Burgos M & Jiménez R. Sox9 and Sox8 protect the adult testis from male-to-female genetic reprogramming and complete degeneration. *eLife* 2016 **5** e15635. (https://doi.org/10.7554/eLife.15635)

27 Hata K, Takahata Y, Murakami T & Nishimura R. Transcriptional network controlling endochondral ossification. *Journal of Bone Metabolism* 2017 **24** 75–82. (https://doi.org/10.11005/jbm.2017.24.2.75)

28 Gonen N, Futtner CR, Wood S, Garcia-Moreno SA, Salamone IM, Samson SC, Sekido R, Poulat F, Maatouk DM & Lovell-Badge R. Sex reversal following deletion of a single distal enhancer of *Sox9*. *Science* 2018 **360** 1469–1473. (https://doi.org/10.1126/science.aas9408)

29 Croft B, Ohnesorg T, Hewitt J, Bowles J, Quinn A, Tan J, Corbin V, Pelosi E, van den Bergen J, Sreenivasan R *et al.* Human sex reversal is caused by duplication or deletion of core enhancers upstream of SOX9. *Nature Communications* 2018 **9** 5319. (https://doi.org/10.1038/s41467-018-07784-9)

30 Malki S, Boizet-Bonhoure B & Poulat F. Shuttling of SOX proteins. *International Journal of Biochemistry and Cell Biology* 2010 **42** 411–416. (https://doi.org/10.1016/j.biocel.2009.09.020)

31 Liu JA, Wu MH, Yan CH, Chau BK, So H, Ng A, Chan A, Cheah KS, Briscoe J & Cheung M. Phosphorylation of Sox9 is required for neural crest delamination and is regulated downstream of BMP and canonical Wnt signaling. *PNAS* 2013 **110** 2882–2887. (https://doi.org/10.1073/pnas.1211747110)

32 Juhász T, Matta C, Somogyi C, Katona É, Takács R, Soha RF, Szabó IA, Cserháti C, Sződy R, Karácsonyi Z *et al.* Mechanical loading stimulates chondrogenesis via the PKA/CREB-Sox9 and PP2A pathways in chicken Micromass cultures. *Cellular Signalling* 2014 **26** 468–482. (https://doi.org/10.1016/j.cellsig.2013.12.001)

33 Reglodi D, Cseh S, Somoskoi B, Fulop BD, Szentleleky E, Szegeczki V, Kovacs A, Varga A, Kiss P, Hashimoto H *et al.* Disturbed spermatogenic signaling in pituitary adenylate cyclase activating polypeptide-deficient mice. *Reproduction* 2018 **155** 129–139. (https://doi.org/10.1530/REP-17-0470)

34 Zákány R, Szucs K, Bakó E, Felszeghy S, Czifra G, Bíró T, Módis L & Gergely P. Protein phosphatase 2A is involved in the regulation of protein kinase A signaling pathway during in vitro chondrogenesis. *Experimental Cell Research* 2002 **275** 1–8. (https://doi.org/10.1006/excr.2002.5487)
35 Tee MK & Miller WL. Phosphorylation of human cytochrome P450c17 by p38alpha selectively increases 17,20 lyase activity and androgen biosynthesis. *Journal of Biological Chemistry* 2013 **288** 23903–23913. (https://doi.org/10.1074/jbc.M113.460048)
36 Kempná P, Marti N, Udhane S & Flück CE. Regulation of androgen biosynthesis – a short review and preliminary results from the hyperandrogenic starvation NCI-H295R cell model. *Molecular and Cellular Endocrinology* 2015 **408** 124–132. (https://doi.org/10.1016/j.mce.2014.12.015)
37 Pandey AV, Mellon SH & Miller WL. Protein phosphatase 2A and phosphoprotein SET regulate androgen production by P450c17. *Journal of Biological Chemistry* 2003 **278** 2837–2844. (https://doi.org/10.1074/jbc.M209527200)
38 Lek M, Karczewski KJ, Minikel EV, Samocha KE, Banks E, Fennell T, O'Donnell-Luria AH, Ware JS, Hill AJ, Cummings BB *et al*. Analysis of protein-coding genetic variation in 60 706 humans. *Nature* 2016 **536** 285–291. (https://doi.org/10.1038/nature19057)
39 de Boer P, Giele M, Lock MT, de Rooij DG, Giltay J, Hochstenbach R & te Velde ER. Kinetics of meiosis in azoospermic males: a joint histological and cytological approach. *Cytogenetic and Genome Research* 2004 **105** 36–46. (https://doi.org/10.1159/000078007)
40 Dudiki T, Kadunganattil S, Ferrara JK, Kline DW & Vijayaraghavan S. Changes in carboxy methylation and tyrosine phosphorylation of protein phosphatase PP2A are associated with epididymal sperm maturation and motility. *PLoS ONE* 2015 **10** e0141961. (https://doi.org/10.1371/journal.pone.0141961)
41 Brosnan PG, Lewandowski RC, Toguri AG, Payer AF & Meyer WJ. A new familial syndrome of 46,XY gonadal dysgenesis with anomalies of ectodermal and mesodermal structures. *Journal of Pediatrics* 1980 **97** 586–590. (https://doi.org/10.1016/S0022-3476(80)80013-8)
42 Loveday C, Tatton-Brown K, Clarke M, Westwood I, Renwick A, Ramsay E, Nemeth A, Campbell J, Joss S, Gardner M *et al*. Mutations in the PP2A regulatory subunit B family genes PPP2R5B, PPP2R5C and PPP2R5D cause human overgrowth. *Human Molecular Genetics* 2019. (https://doi.org/10.1093/hmg/ddy424)
43 Reynhout S, Jansen S, Haesen D, van Belle S, de Munnik SA, Bongers EMHF, Schieving JH, Marcelis C, Amiel J, Rio M *et al*. De novo mutations affecting the catalytic Cα subunit of PP2A, PPP2CA, cause syndromic intellectual disability resembling other PP2A-related neurodevelopmental disorders. *American Journal of Human Genetics* 2019 **104** 139–156. (https://doi.org/10.1016/j.ajhg.2018.12.002)

Received 29 January 2019
Revised version received 14 March 2019
Accepted 20 March 2019